Viscosity Effects on Dean Vortex Membrane Microfiltration

Tanja Kluge, Amrit Kalra, and Georges Belfort
Howard P. Isermann Dept. of Chemical Engineering, Rensselaer Polytechnic Institute, Troy, NY 12180

The influence of changing viscosity by adding polyethylene glycol (PEG) during microfiltration of silica suspensions in the presence and absence of Dean vortices was determined. A new microfiltration membrane module design containing helically wound hollow fibers (with Dean vortices) was compared with a standard commercial cross-flow module (without Dean vortices) containing linear hollow fibers during filtration of poly(ethylene) glycol solutions and silica suspensions. The influence of solution viscosity on permeation flux behavior was evident through two separate effects. First, increased viscosity effected the formation and stability of vortices and, hence, wall shear rate and convective back-flow. Second, permeation flux was reduced with increasing fluid viscosity. Flux improvements (linear vs. helical membranes) of up to 45% were observed for all value of the silica suspensions with and without PEG. The energy required to obtain these improvements, however, was considerable. Flux advantages of the helical design decreased and eventually disappeared as the viscosity of the solution increased up to 12 times that of water at 27°C. New mass-transfer correlations for microfiltration of poly(ethylene) glycol solutions containing silica concentrations for laminar flow in a helical and a linear module were obtained with respect to the solution viscosity, for a silica particle concentration of 0.1 wt. %.

Introduction

An increasing amount of recent evidence, including numerical predictions, stability analysis, and experimental observations, suggests that membrane filtration devices with secondary flow outperform those without such flows (Brewster et al., 1993; Chung et al., 1995, 1998; Wille et al., 1996; Moulin et al., 1996; Bubolz et al., 1998; Luque et al., 1999). Comparisons of performance under conditions of equal energy consumption or equal entrance flow rates always favor the module with secondary flows. These include systems with Taylor Couette or Dean vortex flows (Taylor, 1923; Dean, 1928). Several pressure-driven membrane processes such as microfiltration, ultrafiltration and nanofiltration have been successfully tested under secondary flow conditions for a variety of feeds including salt solutions, macromolecular solutions, and suspensions. The results have been very encouraging garnering commercial interest in the underlying patents (Belfort et al., 1993; Belfort, 1997). In applying new technology such as Dean vortex flows to various filtration applications, it is important to understand the capabilities and the limitations of this new approach. One unknown and unstudied area that has clear relevance to successful applications of Dean vortex flow is the effect of viscosity on performance. In several industries, the viscosity of the feed solution can rise significantly during processing and, especially, during concentration by filtration. How does the Dean vortex filter perform with increasing viscosity? What percent improvement can one expect at high viscosity for the helical (with vortices) vs. the linear (without vortices) modules? How is the axial pressure drop and the difference in axial pressure drop between flow with and without vortices affected by an increase in viscosity? Can one derive a mass-transfer correlation for a range of viscous solutions? The work reported here is an attempt to answer some of these questions for microfiltration of silica suspensions under increasing viscosity in the presence and absence of Dean vortices.

Correspondence concerning this article should be addressed to G. Belfort.
Current address of T. Kluge: Dept. of Chemical Engineering, Technische Universitat Hamburg-Harburg, Germany.

The objective of the work was to separate viscous effects from particle fouling through deposition and cake formation (suspension) during membrane filtration performance. The viscosity of the solutions was varied by the addition of poly(ethylene) glycol (PEG), while the suspension concentration was varied by adding silica (Si) particles with a size distribution between 0.5 and 20 μm and a nominal size of 2.4 μm from 0.1 to 3 wt. % Si particle concentrations. Control experiments to characterize the effect of viscosity on filtration flux behavior and secondary flow for different poly(ethylene) glycol concentrations without silica particles were performed. Then, the effects of particle deposition and cake formation for different silica concentrations in deionized water without poly(ethylene) glycol were studied. Finally, both the effects of viscosity and cake formation were studied with suspensions containing both PEG and silica. New mass-transfer correlations that account for viscosity during microfiltration of poly(ethylene) glycol solutions containing silica concentrations for laminar flow in a helical and a linear module are presented.

Theory

Microfiltration models can be divided into at least two main classes: resistance models and back-flux models. The transmembrane pressure is defined as the difference between the average pressure on the retentate side and the permeate pressure

$$\Delta p_{\mathrm{TMP}} = \frac{p_i + p_o}{2} - p_p \tag{1}$$

where p_i is the feed inlet pressure (kPa, psi), p_o is the retentate outlet pressure, and p_p is the permeate pressure.

When the sieving mechanism of microfiltration is dominant, a cake layer of rejected particles usually forms on the membrane surface (resistance model). The cake layer and the membrane may be considered as two resistances in series, and the pressure driven permeate flux through this cake layer and the membrane is then described at any instant during the microfiltration process by Darcys law

$$J = \frac{1}{A}\frac{dV}{dt} = \frac{\Delta p_{\mathrm{TMP}}}{\eta(R_m + R_c)} \tag{2}$$

The membrane resistance R_m (m^{-1}) can be determined experimentally from the pure water permeability L_p ($\mathrm{L/cm^2h\text{-}kPa}$). In the absence of fouling, R_c can be neglected and the permeate flux J_w ($\mathrm{L/(m^2h)}$) and viscosity of the suspension η are measured at a fixed temperature and pressure

$$R_m = \frac{1}{\eta L_p} = \frac{\Delta p_{\mathrm{TMP}}}{\eta J_w} \tag{3}$$

However, after the start of the experiment, the cake resistance can be expressed as

$$R_c = \frac{\Delta p_{\mathrm{TMP}}}{\eta J_w} - R_m \tag{4}$$

At steady state, the convective flux of material to the membrane is balanced by diffusive back transport for a completely retentive membrane (gel polarization or back-flux model). Then, the flux can be described by

$$J = \left(\frac{D}{\delta_c}\right)\ln\left(\frac{c_w}{c_b}\right) \tag{5}$$

where δ_c (m) is the thickness of the concentration boundary layer, c_w is the concentration at the membrane surface, and c_b is the concentration in the bulk feed. The gel concentration c_w is the concentration at which the solvent flux drops to zero.

The quotient D/δ_c is usually expressed as the mass-transfer coefficient k. The mass-transfer coefficient k (m/s) is a measure of the net mass transfer of solute toward the membrane surface from the bulk solution. This is controlled mainly by fluid-flow conditions and operating temperature. The solute diffusion coefficient D may be calculated from the Stokes-Einstein relationship

$$D = \frac{k^* T}{6\pi\eta r_s} \tag{6}$$

where k^* is the Boltzmann constant ($= 1.380\times10^{-16}$ g $\mathrm{cm^2/s^2K}$), T is the absolute temperature (°C), η is again the dynamic viscosity (Pa·s), and r_s is the radius of the solute particle (cm). The mass-transfer coefficient k ($= D/\delta_c$) can also be estimated from correlations of the Sherwood number $Sh = dk/D$ in terms of the Reynolds number $Re = dv_m/\nu$ and the Schmidt number $S_c = \nu/D$. Generally, mass-transfer correlations are expressed in a dimensionless form such as (Rautenbach, 1997; Zeman and Zydney, 1996)

$$Sh = \alpha Re^b Sc^c \tag{7}$$

where α, b and c are constants often indicative of the flow regime and fluid properties.

Gehlert et al. (1998) proposed a new mass-transfer correlation for ultrafiltration of dextran T500 solutions for laminar flow in a helical hollow fiber module, viz.

$$Sh = 0.173\left(\frac{a}{r_c}\right)^{0.07} Re^{0.55} Sc^{0.33} \tag{8}$$

where a and r_c are the radius and centerline curvature radius of the tube, respectively.

In this study, a mass-transfer correlation, similar in form to Eq. 8, will be presented for poly(ethylene) glycol solutions in Dean vortex and cross-flow flow. The intensity of secondary flow in a curved tube can be described by a dimensionless number called the Dean number (Dean, 1928). The Dean number is usually defined as:

$$De = Re\sqrt{\frac{a}{r_c}} \tag{9}$$

where a is the inner radius of the tube (mm), and r_c is the radius of the curvature of the centerline of the tube (mm).

The Reynolds number Re is defined as usual by

$$Re = \frac{d_i \upsilon_m}{\nu} \tag{10}$$

where υ_m is the mean azimuthal velocity (m/s), d_i ($= 2a$) is the inner diameter of the tube, and ν is the kinematic viscosity (m^2/s) of the fluid. The critical Dean number is defined as the ratio $D = De/De_c$ ($= Re/Re_c$). The curvature ratio $\eta' = (r + a)/(r + a + t)$.

The energy consumption was calculated as the product of axial pressure drop Δp_x ($= p_i - p_o$) for flow along the membrane in the tube and the average axial-flow rate $(Q_i + Q_o)/2$ minus the energy associated with the permeate flow ($Q_p p_p$)

$$E = Q_i p_i - Q_o p_o - Q_p p_p \approx \Delta p_x (Q_i + Q_o)/2 - Q_p p_p \approx \Delta p_x Q_i \tag{11}$$

where $Q_p p_p$ can be neglected and $Q_i \approx Q_o$ for relatively low permeate flow Q_p.

The axial pressure drop due to the friction factor for a straight and a curved tube is generally defined as

$$\Delta p_x = \lambda \frac{l}{d} \frac{\rho}{2} \upsilon_m^2 \tag{12}$$

where l/d is the ratio of length to diameter of the tube, λ is the friction factor, and ρ is the density (kg/m^3) of the fluid. The friction factor for laminar flow in a straight pipe is given by the Hagen-Poiseuille equation

$$\lambda_{\text{linear}} = \frac{64}{Re} \quad \text{for} \quad Re < 2{,}300 \tag{13}$$

Comparing different correlations, Gnielinski (1983) recommended the experimentally obtained correlation for λ_h. The best correlation to predict the friction factor for laminar flow in a helical system is given by Mishra and Gupta (1978)

$$\lambda_h = \frac{64}{Re} \cdot \left[1 + 0.033 \cdot (\log_{10} De)^4\right] \quad \text{for} \quad Re < 5{,}000 \tag{14}$$

As can be seen from a comparison of Eqs. 13 and 14, an additional term in the square brackets is needed for flow in a helical tube. As the curvature or radius ratio a/r_c is decreased, the term in the brackets approaches one, allowing Eq. 14 to approach Eq. 13 suggesting that helical flow becomes similar to linear flow and the influence of secondary flow should disappear.

Experimental

Material

Chemical and Feed Suspensions. Poly(ethylene) glycol (Sigma Chemical Co., St. Louis, MO, No. P6667, 99%) with an average molecular weight of 10 kDa and a density of 1,070 kg/m^3 was dissolved in DI water to vary the solvent viscosity between 1 and 15 wt. %. Addition of silica particles (Sigma Chemical Co., St. Louis, MO, No. S5631, 99%) was used to vary the suspended particle concentration. The particle diameter distribution was approximately between 0.5 and 10 μm with 80% between 1 to 5 μm. The particle-size distribution is shown in Figure 1. The mean particle diameter was determined to be 2.4 μm. NaOH (Sigma Chemical Co., St. Louis, MO, No. S5881, 98%) and NaOCl solutions (Aldrich Chemical Company Inc., Milwaukee, WI, No. 22,930-5) were used to clean the membranes.

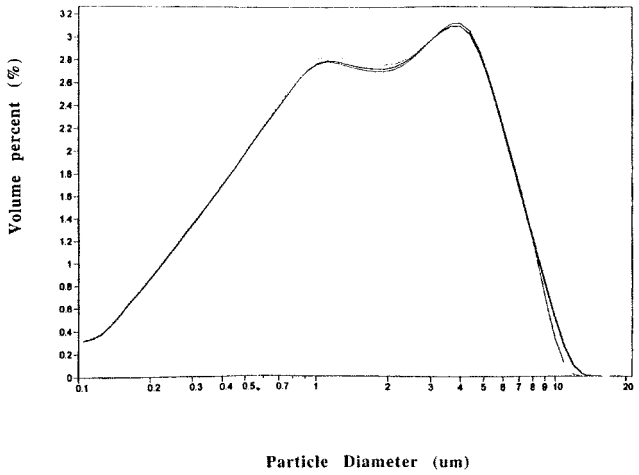

Figure 1. Particle-size distributions for silica based on volume percent.

Membrane Modules. The two membrane modules used in this work were tubular hollow fiber modules and were produced by Millipore Corp. (Module No. 082997-1/3, prototype, Bedford, MA). Each module had six 0.1 μm mean pore-size poly(sulfone) hollow fibers. For the helical module, the fibers were wound in a single-wrap helix around an acrylic rod (Figure 2). The purpose of the rod was to stabilize the membrane helix and establish the desired curvature (a/r_c). The linear module was constructed for standard crossflow. Table 1 summarizes the specifications and operation parameters for the helical and linear module.

Methods

Flowsheet. Figure 3 shows the flow diagram of the microfiltration pilot-plant system. This system consisted of two parallel flow lines, which allowed one to compare the two mod-

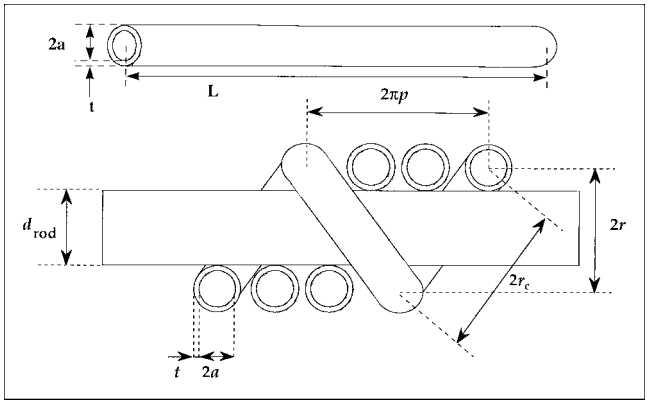

Figure 2. Linear and helical hollow fiber configurations.

Table 1. Design Specification and Operating Characteristics of Microfiltration Membrane Modules*

Property	Linear (No. 082997-4)	Helical (No. 082997-1)
Length of module, L_{module} (mm)	410	160
Dia. of module, D_{module} (mm)	30	30
No. of fibers, m	6	6
Active fiber length, l_{fiber} (mm)	342.9	317.5
Fiber ID, $2a = d_I$ (mm)	0.835	0.835
Fiber OD, d_o (mm)	1.57	1.57
Memb. surface area, A_m (cm^2)	65	60
Rod dia., d_{rod} (mm)	—	6.35
Radius of curvature, r_c (mm)	—	4.45
Radius ratio, a/r_c	—	0.1
Radius ratio, $\eta' = r_1/r_2$	—	0.82
Critical Reynolds No., Re_c	—	45.8
Critical Dean No., De_c	—	14.31
Pitch, p (mm)	—	1.45
Curvature, κ (L/mm)	—	0.224
Torsion, τ (L/mm)	—	0.082
Operation pH	2–12	2–12
Max. temp. (°C)	60	60
Pore size (μm)	0.1	0.1

*Built by Millipore Corp., Bedford, MA.

ules, the linear and the helical module, simultaneously. For a further description, see earlier literature (Luque et al., 1999; Gehlert et al., 1998).

System Preparation. Prior to each experiment, the sodium hydroxide (NaOH, 5 g/L, pH 12.5) in which the membranes were stored was washed from the modules by passing DI water through the system. A water permeability test (permeate flux vs. transmembrane pressure) was conducted before each experiment. If the water permeability was too low, an additional cleaning procedure was initiated. The cleaning procedure was repeated until the water permeability was constant.

Constant Transmembrane Pressure Experiments. Each experiment was run at the same entrance flow rate and transmembrane pressure for both modules. The maximum transmembrane pressure (measured as $p_{in} - p_{permeate}$) was maintained below 68 kPa (10 psi) in order to minimize membrane compaction and fouling and to prevent fiber collapse (Luque et al., 1999). First, the valves to the tubes of the helical and linear module were opened (the permeate valves were kept closed). The retentate outlet valves were opened completely and the desired inlet pressure was established. The initial axial-flow rate, measured with these settings, was the highest possible axial-flow rate for the experiment, due to the clean unused membrane. Then, to prevent unwanted fouling due to a large initial permeate flux, the permeate outlet valves were opened slowly until the desired TMP was reached. After TMPs and flow rates were readjusted, the experiments were started with a stabilization period at these operating conditions (highest flow rate), until steady-state flux was reached, that is, the permeate flow rates remained constant with time. This permeate flow value was recorded for the highest axial-flow rate. Then, the feed flow rates in both modules were decreased step by step in order to obtain data at lower flow rates. Next, the permeate flow rates were recorded for each axial-flow rate. The permeate was recycled back to the feed tank, so that the feed concentration remained constant during the whole experiment.

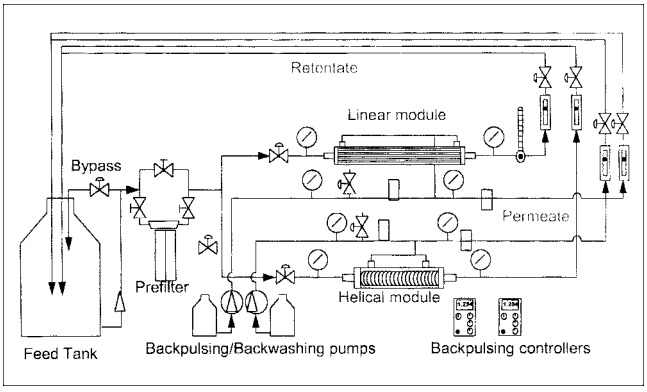

Figure 3. Flow sheet for microfiltration pilot plant (Gehlert, 1998).

Cleaning Procedure. The modules were back- and forward-washed with 1 L (for the low PEG experiments) and up to 5 L (for high PEG experiments) of DI water at 40°C, respectively. When the feed solution contained silica particles, the modules were back- and forward-washed with 1 L and 4 L of a 5 g/L NaOH solution, respectively. Additionally, the modules were placed in NaOH solution for 30–60 min. Then the NaOH solution was washed out of the system by back- and forward-washing with deionized (DI) water, followed by back- and forward-washing with 1 L and 4 L of a 0.5 mL/L bleach solution, respectively. Finally, for each experiment, the system was rinsed completely with DI water (back- and forward-washing) and an additional water permeability check with pre-filtered DI water was obtained.

Results and Discussion

Poly(ethylene) glycol (experiments)

By choosing 10 kDa PEG, with zero retention, the influence of concentration polarization and fouling was minimized. Thus, the effect of solution viscosity on the flux behavior and on the formation and stability of the Dean vortices could be studied. The effect of particle deposition on flux behavior and secondary flow is discussed below. However, for the case of minimal concentration polarization and fouling, both modules helical and linear, exhibited approximately the same flux behavior for the range of viscosities studied.

Effect of Viscosity on Flux Behavior. Figure 4 shows the permeate fluxes as a function of Reynolds number (Re) and Dean number ratio (D) for different poly(ethylene) glycol concentrations (such as different viscosities). A correlation between PEG concentration and relative viscosity η_r ($= \eta/\eta_o$, where η_o = viscosity of water at 25.5°C) for different temperatures was obtained by Kluge (1998). Using a power relationship

$$\eta_r = 1 + a'c + b'c^2 \qquad (15)$$

she obtained $a' = -0.0911$ and $b' = 0.058$ at 25.5°C with $R^2 = 0.9979$. c is the PEG concentration is wt. %. With increas-

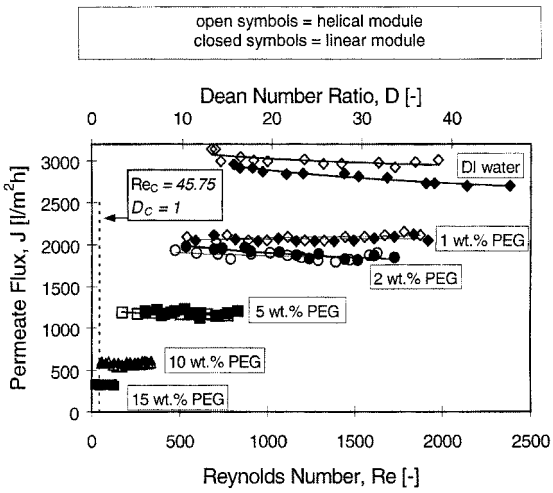

Figure 4. Permeate flux vs. Reynolds number for different poly(ethylene) glycol concentrations.

c = 0–15%; TMP = 27.58 kPa (4 psi); T = 24.5–27.5°C.

ing the PEG concentration and, hence, viscosity, the permeate flux dropped significantly compared to the DI water flux for both modules. According to the resistance model (Eq. 2), the permeate flux should be a function of the inverse dynamic viscosity. Also, due to the definition of *Re*, which is a function of the inverse dynamic or kinematic viscosity (Eq. 10), the operational range of *Re* decreased for the same axial-flow rate range due to increasing viscosity. Because PEG was not retained, the permeate fluxes were independent of the *Re* and similar for both modules. Therefore, a flux improvement for the helical module compared to the linear module was, as expected, not observed. Table 2 shows the average values of the permeate fluxes for both modules as a function of the PEG concentration and viscosity.

Membrane Resistance. As expected, the resistance model was in good agreement with the decrease in permeate flux. Figure 5 shows the arithmetic average of the permeate flux values for different poly(ethylene) glycol concentrations from Figure 4 as a function of the inverse viscosity. Using the slope of the linear lines for both modules in this plot, the membrane resistance (R_m) was calculated according to the resistance model (Eq. 3). In the absence of fouling, R_c can be neglected. The permeate flux and solution viscosity were measured:

$$R_m = \frac{\Delta p_{\mathrm{TMP}}}{(\mathrm{slope})} = 4.064\times 10^{10}\ (\mathrm{linear})\ \text{and}$$

$$4.042\times 10^{10}\ (\mathrm{helical})\ [\mathrm{m}^{-1}]. \quad (16)$$

The membrane permeability as a function of solution viscosity can be determined by the Hagen-Poiseuille equation. Since the PEG was freely transmitted through the membranes, it does not polarize nor exhibit an osmotic pressure difference. Both modules were equivalent throughout the permeate flux range

$$L_{pi} = \frac{J_i}{\Delta p_{\mathrm{TMP}}} = \frac{1}{\eta_i \cdot R_m} \quad [\mathrm{l/m^2\ h\ kPa}] \quad \Delta\Pi = 0 \quad (17)$$

Table 2. Average Permeate Flux and Membrane Permeability for Liner and Helical Module as a Function of PEG Concentration (such as Viscosity)

PEG Conc. (wt. %)	Vis.* (Pa·s)	Av. $J_{P,\mathrm{linear}}$ † (L/m²·h)	Av. $J_{P,\mathrm{helical}}$ † (L/m²·h)	$L_{Pj,\mathrm{linear}}$ ‡ (L/m²·h·kPa)	$L_{Pi,\mathrm{helical}}$ ‡ (L/m²·h·kPa)
0	0.00085	2805.0	3043.9	101.71	110.37
1	0.00098	2067.5	2087.4	74.97	75.68
2	0.00104	1895.2	1867.5	68.72	67.71
5	0.00199	1184.7	1165.5	42.95	42.26
10	0.00459	593.2	571.7	21.51	20.73
15	0.01257	324.3	330.3	11.76	11.98

*Obtained as an arithmetic average from viscosity measurements during constant TMP experiments at 4 psi.
†Obtained as an arithmetic average from permeate flux measurements during constant TMP experiments at 27.58 kPa (4 psi).
‡Obtained from Eq. 3.

Table 2 summarizes the results of membrane permeabilities as a function of PEG concentration (such as viscosity). The permeabilities decreased with increasing viscosity.

Effect of Viscosity on Energy Consumption. To compare the energy consumption for both modules, the total energy consumption for each module was divided by the membrane area and plotted as a function of Reynolds numbers (Figure 6a). These data clearly show that, at a low PEG concentration (such as low viscosity), the energy consumption increased mainly as a function of *Re* (and, therefore, as a function of the axial-flow rate to the second power for laminar flow). Also, the helical module had higher energy consumption per membrane area than the linear one, due to the presence of secondary flow, that is, formation of Dean vortices. However, these differences narrow considerably at high viscosities because the energy consumption was dominated by solution viscosity. With increasing PEG concentration, the difference in energy consumption between the helical and the linear modules decreased and was very small for a PEG concentration of 15 wt. %. One explanation for this observation is that the Dean vortices became weaker with increasing solution viscosity and, therefore, the difference in the energy consumption for the helical and linear modules decreased. Also, the *Re*

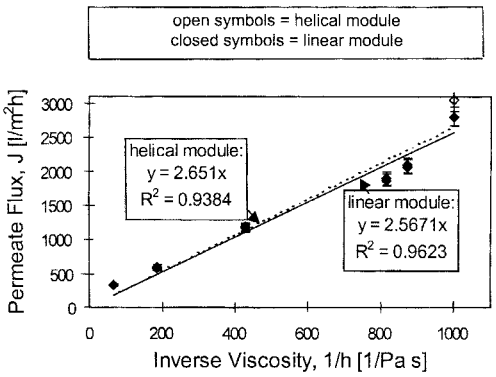

Figure 5. Permeate flux vs. inverse dynamic viscosity of poly(ethylene) glycol.

The data for the permeate fluxes and viscosities are average values taken from Figure 4 and Table 2. (TMP = 27.58 kPa (4 psi); T = 24.5–27.5°C.)

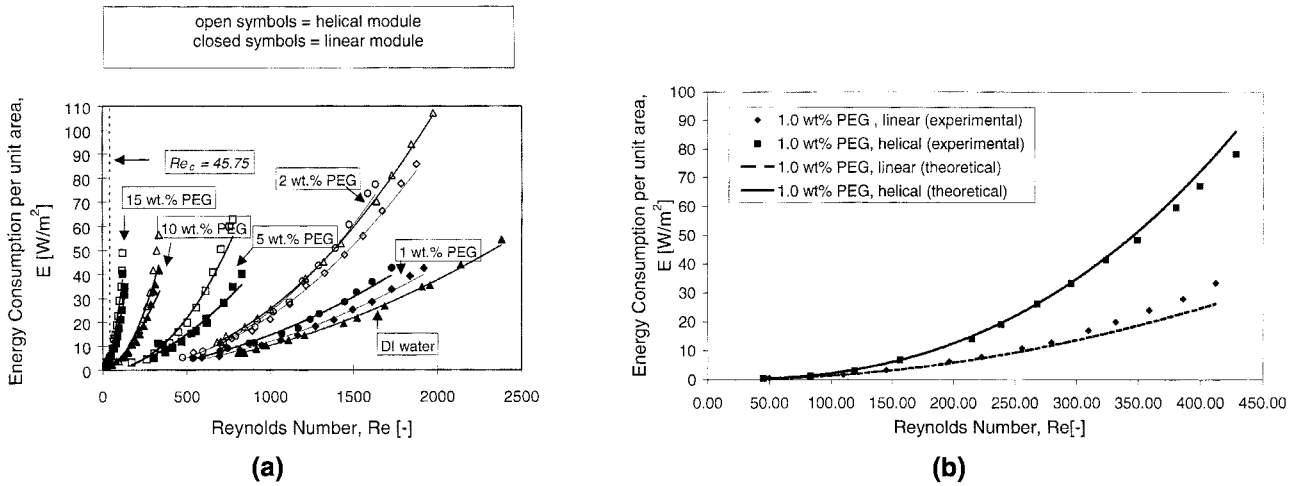

Figure 6. Energy consumption per unit area vs. Reynolds number.

For (a) different poly(ethylene) glycol concentrations ($c = 0$–15.0 wt. %, TMP = 27.58 kPa (4 psi), $T = 24.5$–27.5°C); (b) comparison of the theory and the measurements for 1 wt. % PEG. Fiber length and inner fiber diameter were taken from Table 1. $\rho = 1{,}070$ kg/m^3 and $\mu = 0.000926$ kg/(m·s).

range decreased with increasing viscosity for the same axial-flow operating range of the axial-flow rate, as mentioned earlier with respect to Figure 4. Substituting λ from Eqs. 13 and 14 into Eq. 12 for the axial pressure drop and then into Eq. 11, the energy consumed per unit area was calculated and compared with the experimental measurements for a 1 wt. % PEG solution (Figure 6b). Satisfactory agreement is observed.

In order to clearly show that the difference in energy consumption decreases with increasing PEG concentration, the ratio of energy consumption for the helical to the linear module was plotted as a function of axial volumetric flow rate (Figure 7), respectively. With increasing PEG concentration from 1 to 15 wt. %, the energy ratio dropped from about 2.2 to 1.0, due to the higher viscosity of the solution. Increasing viscosity seemed to have an effect on Dean vortices in the helical module. A likely explanation is that with increasing viscosity the *Re* decreases and approaches or falls below the critical Re_c, thus severely weakening the vortices. In Figure 7b, the prediced energy consumption ratio overshoots the measurements for a 1 wt. % PEG solution.

Silica experiments

Silica particles with a mean particle diameter of 2.4 μm were added to DI water as the feed suspension in order to study the effect of suspension concentration on flux behavior, and the formation and stability of Dean vortices in the absence of PEG. The silica particles were completely retained by the microfiltration membrane (mean pore size: 0.1 μm)

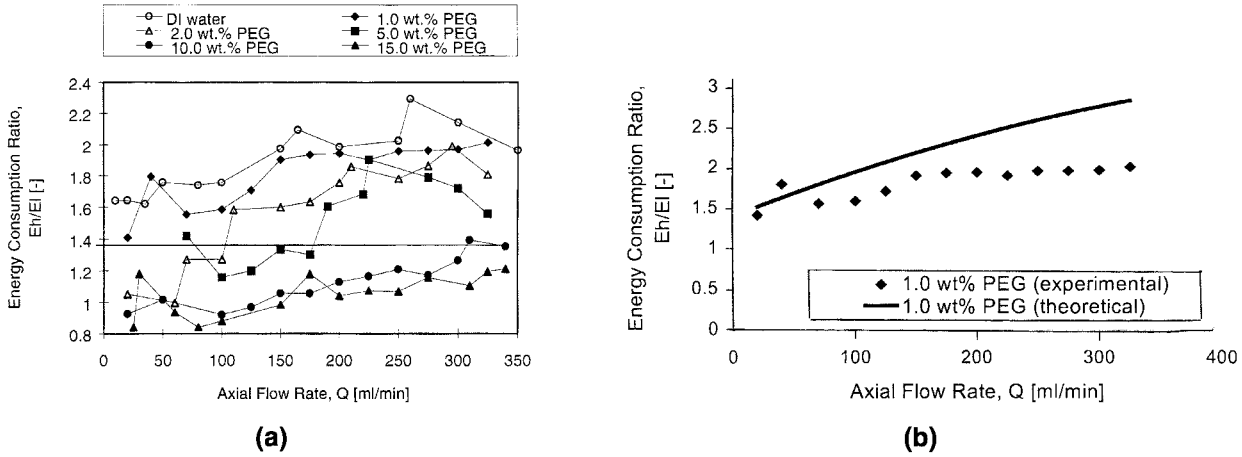

Figure 7. Ratio of the energy consumption per unit area for the helical module to the linear module vs. axial-flow rate.

For (a) different poly(ethylene) glycol concentrations.($c = 0$–15.0 wt. %, TMP = 27.58 kPa (4 psi), $T = 24.5$–27.5°C); (b) comparison of the theory and the measurements for 1 wt. % PEG. Fiber length and inner fiber diameter were taken from Table 1. $\rho = 1{,}070$ kg/m^3 and $\mu = 0.000926$ kg/(m·s).

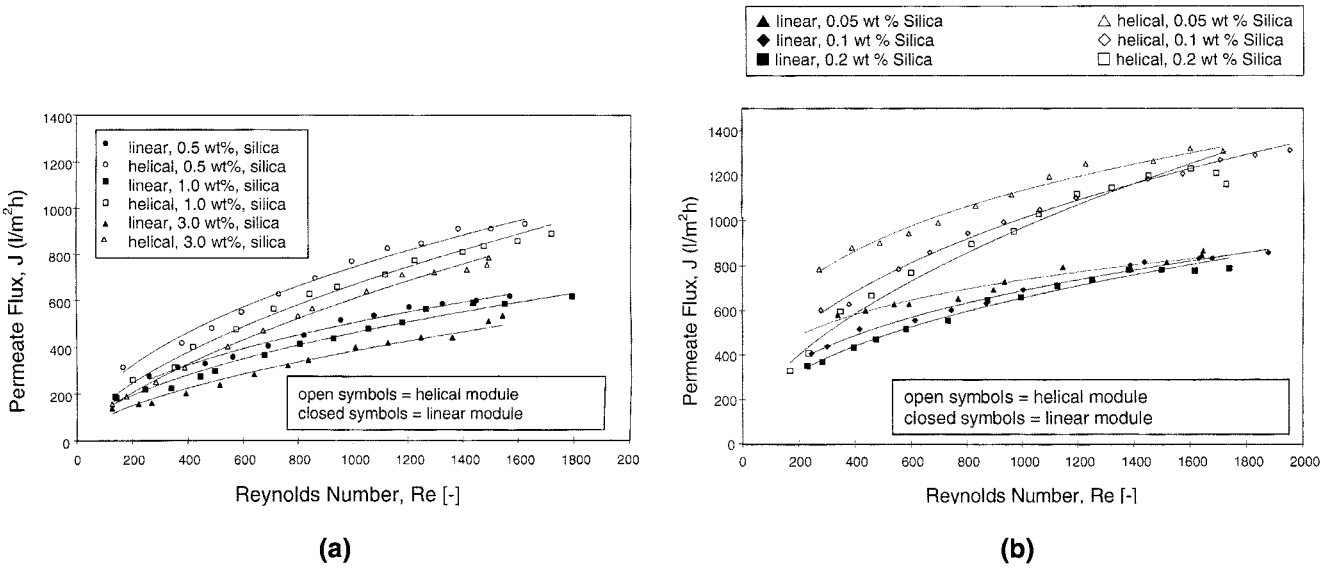

Figure 8. Permeate flux vs. Reynolds number for different silica concentrations.

(a) $c = 0.05-0.2$ wt. %; (b) $c = 0.5-3.0$ wt. %. Open symbols represent data for the helical module and closed symbols represent the data for the linear module. (TMP = 27.58 kPa (4 psi), $T = 27°C$.)

and, therefore, formed a deposit layer on the membrane surface. Viscosity effects through addition of silica particles on the feed solution were minor for these experiments (Kluge, 1998). With a maximum concentration of suspended silica of 3.0 wt. %, the estimated suspension viscosity was 0.000912 Pa·s, as compared to 0.000855 Pa·s for pure water (at 25°C); approximately a 7% increase.

Effect of Feed Flow Rate and Silica Concentration. The presence of silica particles decreased the solvent flux for both modules due to the formation of cake layer on the membrane. Figure 8 shows the permeate flux for different silica concentrations (0.05–3.0 wt. %) as a function of Reynolds number. The flux behavior, however, was completely different from that of PEG (Figure 4). For silica particles, the permeate flux was a function of Reynolds number and increased with increasing *Re* in the typical *concave* shape for microfiltration. The flux was highest at low silica concentrations and high *Re*, and decreased with increasing silica concentrations and decreasing Re. The permeate flux dropped dramatically compared to the pure water flux with the addition of a small amount of silica particles to the feed solution. For example, the permeate flux dropped about 55% (helical) and 73% (linear) for a silica concentration of 0.1 wt. % ($J_w = 3{,}000$ L/m^2 h (pure water) compared to $J_{s,\text{helical}} = 1{,}400$ L/m^2·h and $J_{s,\text{linear}} = 800$ L/m^2·h at $Re = 2{,}000$). To improve the permeate flux in a linear module, it is necessary to increase the cross-flow velocity and, hence, the wall shear stress. The higher cross-flow velocity reduced the deposit layer buildup by resuspending the particles back into the bulk stream. In the helical module both the presence of secondary flow and the wall shear stress due to the cross-flow velocity were operable. These vortices induced a back convective flow away from the membrane thereby reducing cake buildup and forming a thinner cake layer compared to the linear module. Due to secondary flow, the permeate flux for the helical module was much higher than that for the linear module. The effect of Dean vortices on deposit layer buildup and, therefore, deposit resistance is discussed separately below.

Effect on Flux Improvement. To show the increase of the permeate flux for different silica concentrations in the helical module over that in the linear module, the percent improvement was plotted against the *Re* in Figure 9. The flux improvements for all silica concentrations increased with increasing *Re* reaching an asymptote of $45 \pm 10\%$ above a *Re* of about 600 ($Q > 150$ mL/min), where the improvements were independent of silica concentration and *Re*. A decrease in flux improvement mentioned by Gehlert et al. (1998) with

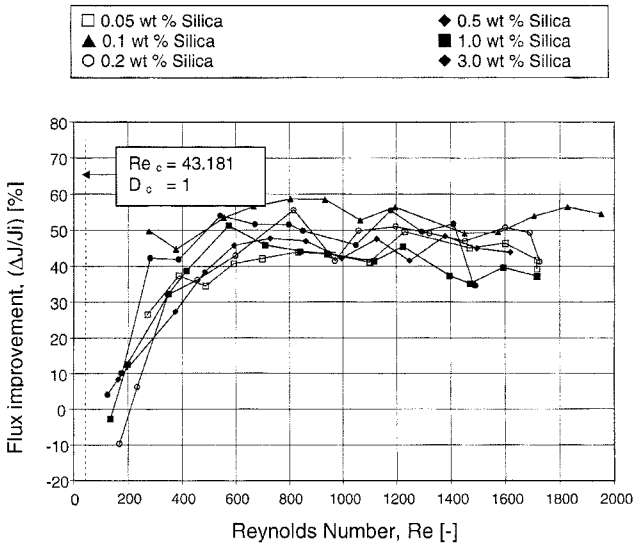

Figure 9. Flux improvement vs. Reynolds number for different silica concentrations.

$c = 0.05-3.0$ wt. %, TMP = 27.58 kPa (4 psi), $T = 27°C$.

dextran solutions at high *Re* was not obvious. Rautenbach (1997) also reported that there is an optimum axial-flow rate for ultrafiltration, because above this flow rate, the permeate flux decreases due to pressure losses along the flow path. Because of secondary flow, the pressure losses are higher in the helical module than in the linear module (Figure 10). There appears to have been a jump in axial pressure drop with increasing silica concentration from 1 to 3 wt. % for both helical and linear modules. The feed pressure and, therefore, the transmembrane pressure in the helical module probably decreased strongly in the first few coils, especially when the axial pressure drop is very high at high flow rates (Ramshankar and Sreenivasan, 1998). This jump was not accounted for in the predictions and, hence, the equations under predict the axial pressure drop at 3 wt. % of silica. For 0.5 wt. % silica, the predictions are relatively good for the helical module, but less so with the linear module.

Effect on Energy Consumption. Since energy consumption depends strongly on viscosity, as shown above for PEG solutions, the energy consumption for the silica suspensions was independent of the silica concentration, as shown in Figure 11 (except for the 3 wt. % suspension). Variation of silica concentration from 0.05 to 1.0 wt. % in aqueous solutions does not substantially effect on the suspension viscosity. The theoretical curves in Figure 11 show the typical *concave* shape for microfiltration. Again, the prediction for the helical module is better than that for the linear module. Due to secondary flow, the energy consumption in the helical module was, as expected, higher than that for the linear module. The energy consumption also increased with Reynolds number. Figure 12 shows the ratio of the energy consumption for the helical module over that for the linear module as a function of *Re* for different silica concentrations. However, for $Re > 1{,}000$ ($Q > 250$ mL/min), the energy ratio reached a constant level about 2.15, that is, the helical module consumed 115% more energy than the linear module.

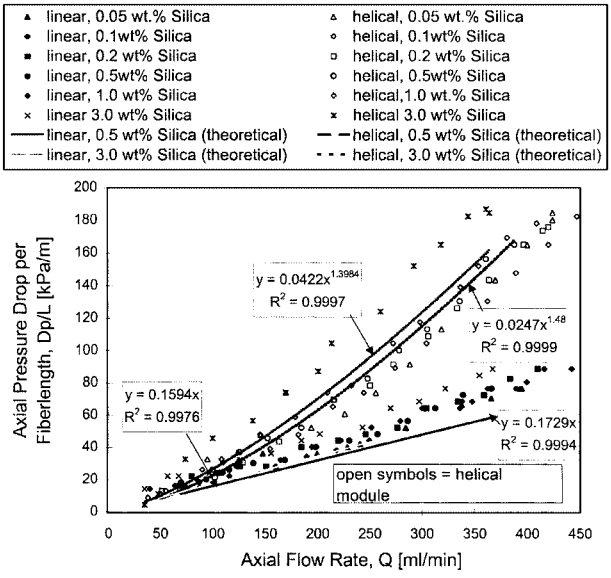

Figure 10. Axial pressure drop per fiber length vs. axial-flow rate for different silica concentrations.

Open symbols represent data for the helical module and closed symbols represent the data for the linear module. ($c = 0.05$–3.0 wt. %, TMP = 27.58 kPa (4 psi), $T = 27$°C.) The theoretical lines are for 0.5 and 3.0 wt. % silica for the helical and linear modules.

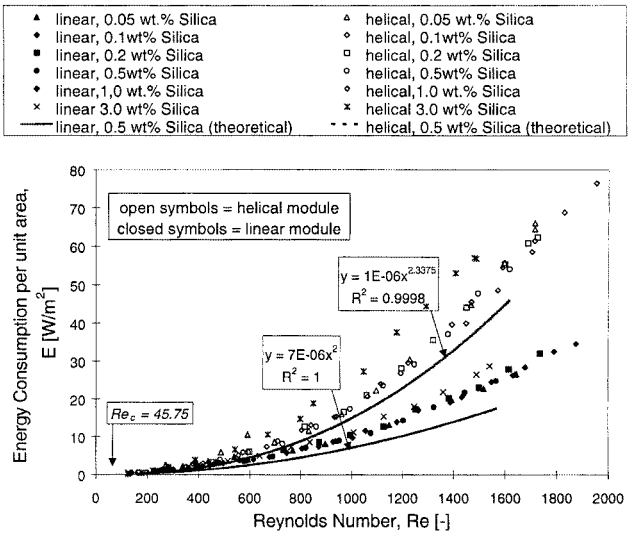

Figure 11. Energy consumption per unit area vs. Reynolds number for different silica concentrations.

Open symbols represent data for the helical module and closed symbols represent data for the linear module. ($c = 0.05$–3.0 wt. %, TMP = 27.58 kPa (4 psi), $T = 27$°C.) The theoretical lines are 0.5 wt. % silica for the helical and linear modules.

To compare the performance of the helical modules with that of the linear modules, the ratio (helical over linear) of energy consumption and permeate flux were plotted against *Re* (Figure 12a). With increasing axial-flow rate, hence, *Re*, both flux and energy ratios increased and reached asymptotes for *Re* greater than 600 (flux) and 1,000 (energy), respectively. This plot clearly shows that the higher permeate flux of the helical module is compensated for by the higher energy consumption of the helical module. The value of the energy ratio was about 2.1 times higher than the value of the flux ratio. The theoretical prediction for the energy ratio is shown for 0.5 wt. % silica. At higher Reynolds numbers, it overshoots the data somewhat. Another plot (Figure 12b) shows the previous results in percent flux improvement as a function of percent energy consumption factor for different silica concentration. Most data points lay in the upper right quadrant. This indicates a positive flux improvement of the helical module over the linear module, but also a higher energy consumption of the helical compared to the linear one. Conditions at low flow rate (< 100 mL/min) or low *Re* (< 300) exist in which higher flux ratios than energy ratios were possible (that is, above the diagonal). This was also the case where a positive $\Delta J/J_{\text{lin}}$ was associated with a negative $\Delta E/E_{\text{lin}}$. For applications in which energy costs are important (water and wastewater), operation at low axial-flow rates with 5–30% flux improvement and lower energy consumption are recommended.

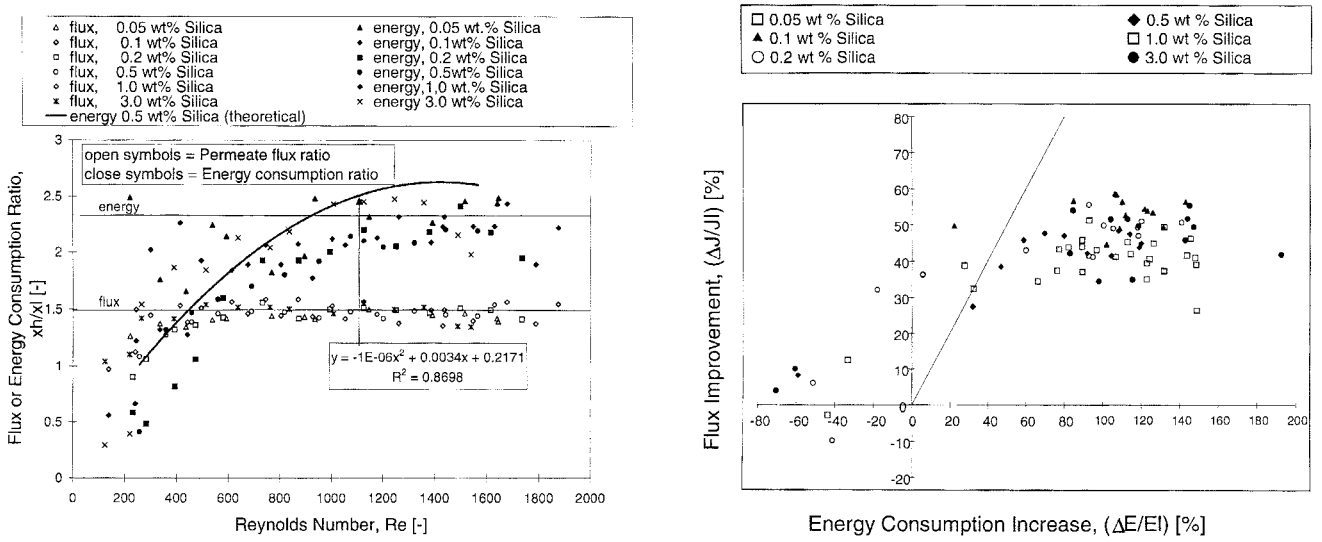

(a) (b)

Figure 12. (a) Ratio of permeate flux and energy consumption for the helical module to the linear module vs. Reynolds number for different silica concentrations (theoretical line is for 0.5 wt. % silica for the energy consumption ratio); (b) flux improvement vs. energy consumption factor for different silica concentrations.

c = 0.05–3.0 wt. %, TMP = 27.58 kPa (4 psi), T = 27°C.

Total Deposit Resistance. For silica suspensions, the total deposit or cake resistance decreased with increasing *Re* in a convex shape (data not shown). The resistance as a function of *Re* was highest for the highest silica concentration and at low *Re*, and decreased with decreasing silica concentration and increasing *Re*. For a constant *Re*, the resistance of the deposit for the linear module was higher than that for the helical module at all silica concentrations due to the additional presence of secondary flow in the helical module. To compare the deposit resistances directly, for both modules, the resistance ratio (helical over linear) was plotted against the *Re* (data not shown). With increasing *Re*, the ratio decreased from about 1 near the critical *Re* to 0.57 ± 0.04, and was constant for *Re* greater than about 500 for all concentrations within a 10% experimental error. This suggests that the effectiveness of Dean vortices in reducing fouling was inde-

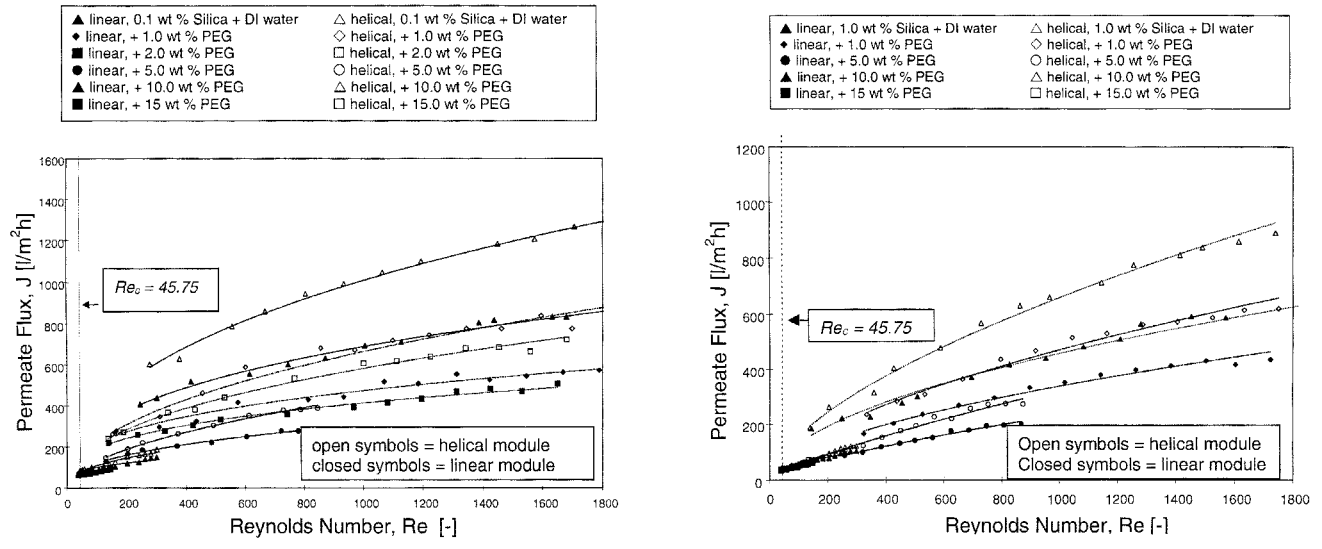

(a) (b)

Figure 13. Permeate flux vs. Reynolds number for different poly(ethylene) glycol solutions (c = 0–15.0 wt. %) containing (a) 0.1 wt. % and (b) 1.0 wt. % silica concentrations.

Open symbols represent data for the helical module and closed symbols represent the data for the linear module. (TMP = 27.58 kPa (4 psi), T = 27°C.)

pendent on the silica particle concentration for $Re > 500$. As will be shown later, the intensity of Dean vortices was effected by solution viscosity. As mentioned above, the range of silica concentration (at least below 3 wt. %) did not effect the solution viscosity.

Silica and PEG experiments

In this section the effect of Dean vortices on microfiltration performance of different PEG (such as different viscosities) solutions containing different suspended silica concentrations is discussed. The results will be compared with those reported earlier for microfiltration of different PEG solutions without silica and aqueous suspensions of silica without PEG.

Effect of Feed Flow Rate and Silica and PEG Concentration on Flux Behavior. The presence of silica particles decreased solvent flux for both linear and helical modules, as shown above. Increasing the solvent viscosity (via the PEG concentration) amplified this effect. Figure 13 shows the permeate fluxes for different poly(ethylene) glycol concentrations as a function of *Re*. The PEG solutions contained 0.1 and 1.0 wt. % suspended silica in Figures 13a and 13b, respectively. The flux behavior of these mixtures follows the flux behavior of the silica suspension since the silica and not the PEG caused fouling. For PEG solutions containing suspended silica, the permeate flux was a function of *Re* and increased with increasing *Re* in a typical *concave* shape for microfiltration. The flux was highest at low silica concentration, low viscosity, and high *Re*, and decreased with increasing silica concentration, increasing viscosity and decreasing *Re*. The permeate flux drop was significant with increasing viscosity of the solution for both modules as compared with the permeate flux in the absence of PEG. For example, the permeate flux dropped about 55% (helical) and 63% (linear) for a silica concentration of 0.1 wt. % with increasing viscosity of about 5 times. ($J_{0,\text{helical}} = 870$ L/m^2·h and $J_{0,\text{linear}} = 600$ L/m^2·h compared to $J_{s,\text{helical}} = 390$ L/m^2·h and $J_{s,\text{linear}} = 220$ L/m^2·h for $Re =$ 600.) Due to secondary flow, the permeate fluxes of the helical module were higher than those in the linear module. Also the *Re* operation range decreased for the same axial-flow rate range due to increasing viscosity as previously mentioned for Figure 4.

Effect on Flux Improvement. Figures 14a and 14b show the flux improvement for different poly(ethylene) glycol concentrations containing 0.1 and 1.0 wt. % silica concentrations as a function of axial-flow rate, respectively. The highest value of flux improvement was observed for aqueous silica suspensions without PEG. The flux improvement decreased for silica suspensions with increasing PEG. For silica suspensions with low PEG concentrations (such as low viscosity), the flux improvement was mostly a function increased axial-flow rate (hence, *Re*) until reaching an asymptote. For *Re* greater than 1,000 ($Q > 250$ mL/min), the flux improvement was relatively constant at 50% and 40% for aqueous solutions containing 0.1 and 1.0 wt. % silica concentrations within experimental errors, respectively. This behavior was similar to that observed with aqueous silica suspensions without PEG as described above and in Figure 9. While for silica suspensions with increasing PEG concentrations, the influence of Dean vortices on flux improvement became weaker in reducing the buildup of deposit on the membrane. Therefore the increase in flux improvement was smaller at high viscosities. Also, the *Re* operation range decreased for the same axial-flow rate range due to increasing viscosity as previously mentioned for Figure 4. For PEG concentrations of 15 wt. % (such as $\eta \approx$ 0.012 Pa·s), the flux improvement was close to zero. A possible explanation for the constant improvement observed at high axial-flow rates or *Re* is related to the effectiveness of the Dean vortices to re-entrain the deposit particles from the membrane.

Effect of Energy Consumption. In order to compare the energy consumption for fluid flow through both modules, the energy consumption was divided by the membrane area and plotted as a function of Reynolds numbers for different PEG concentrations containing silica concentrations. The energy

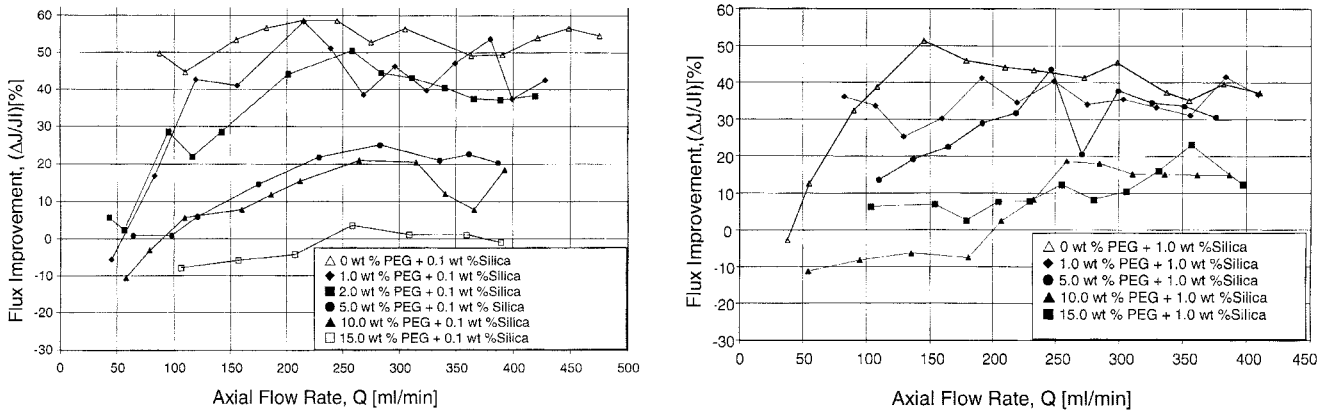

Figure 14. Flux improvement vs. axial-flow rate for different poly(ethylene) glycol solutions (c = 0–15.0 wt. %) containing (a) 0.1 wt. % and (b) 1.0 wt. % silica concentrations.

Open symbols represent data for the helical module and closed symbols represent the data for the linear module. (TMP = 27.58 kPa (4 psi), $T = 27$°C.)

consumption was mainly a function of viscosity, and addition of silica particles had no noticeable effect on the solution viscosity (as shown above, no effect on the energy consumption behavior was observed by addition of silica concentrations up to 1.0 wt. %). Hence, the energy consumption behavior for PEG solutions containing silica particles was similar to those of PEG solutions without silica particles (data not shown, for 0.1 and 1 wt. % silica concentrations, they were similar to those in Figure 6). With respect to the energy behavior of PEG solutions with and without silica particles, the ratio of energy consumption for the helical to the linear module were plotted as a function of total axial-flow rate. Although the results are not shown here, they were similar to those in Figure 7 for PEG solutions without silica in the solutions. With increasing PEG concentrations from 1 to 15 wt. %, the energy ratio dropped down from 2.3 to 1.0 in the presence of 1.0 wt. % silica particles (data not shown) and from 2.0 to 1.0 in the absence of silica particles (Figure 7), in both cases due to the increased viscosity. The presence of silica particles seemed to have little or no effect on energy behavior since viscosity did not perceptibly change with silica particles in the feed. As before, increasing viscosity appears to have an effect on Dean vortices in the helical module. As the solution or suspension viscosity increases to large values, the additional energy needed to pump fluid through the helical tube approximates that needed for the linear tube. It is likely that at this point, the centrifugal vortices have difficulty forming or are weak.

In order to compare the performance of the helical modules with that of the linear modules, flux improvement ($\Delta J/J_{lin.}$) for different poly(ethylene) glycol concentrations (such as different viscosities) was plotted against the energy consumption factor ($\Delta E/E_{lin.}$) (Figure 15). These PEG solutions contained 0.1 wt. % and 1.0 wt. % silica particles. These plots show clearly that the higher flux improvement of the helical modules is compensated for by the higher energy consumption as compared with the linear modules. Only at low axial-flow rates, the energy consumption factor is less than the flux improvement. Of course, for some industries, such as the pharmaceutical, biotechnology, or food and beverage industries, a 40–60% increase in permeation flux may far outweigh the additional operation costs of 80–130% increase in pumping energy. Thus, as stated before, with the silica suspensions (without PEG), operation was at low flow rates or *Re* and with dilute suspensions at low viscosities; flux improvement was higher than the energy consumption factor (Figures 15a and 15b).

Effect of Viscosity on Total Deposit Resistance and Dean Vortices. The total deposit resistance for 0.1 wt. % and 1.0 wt. % silica concentrations and different PEG concentrations as a function of Reynolds number (data not shown). At all PEG concentrations, the deposit or cake resistance for the linear module was higher than that for the helical module at a given Reynolds number for both silica concentrations. The difference in the cake resistance narrowed with increasing viscosity. Further, the resistance decreased with increasing Reynolds number and showed a similar *convex* shape as mentioned earlier for silica suspensions without PEG. At low PEG concentrations (such as low viscosity), the effect of solution viscosity on cake resistance and on secondary flow were small and the resistance behavior was similar to those of silica suspensions without PEG. However, at higher PEG concentrations, the effect of viscosity on Dean vortices and, therefore, on particle deposit resistance behavior became stronger, due to weaker Dean vortices. The deposited particle layer resistance decreased significantly for both modules. Also, the *Re* operating range decreased with increasing viscosity for the same axial-flow rate range as mentioned previously with Figure 4. Further, to illustrate the behavior between the resistance of both linear and helical modules, the total resistance ratio of the helical to the linear module was plotted against axial-flow rate instead of *Re*, so as to remove

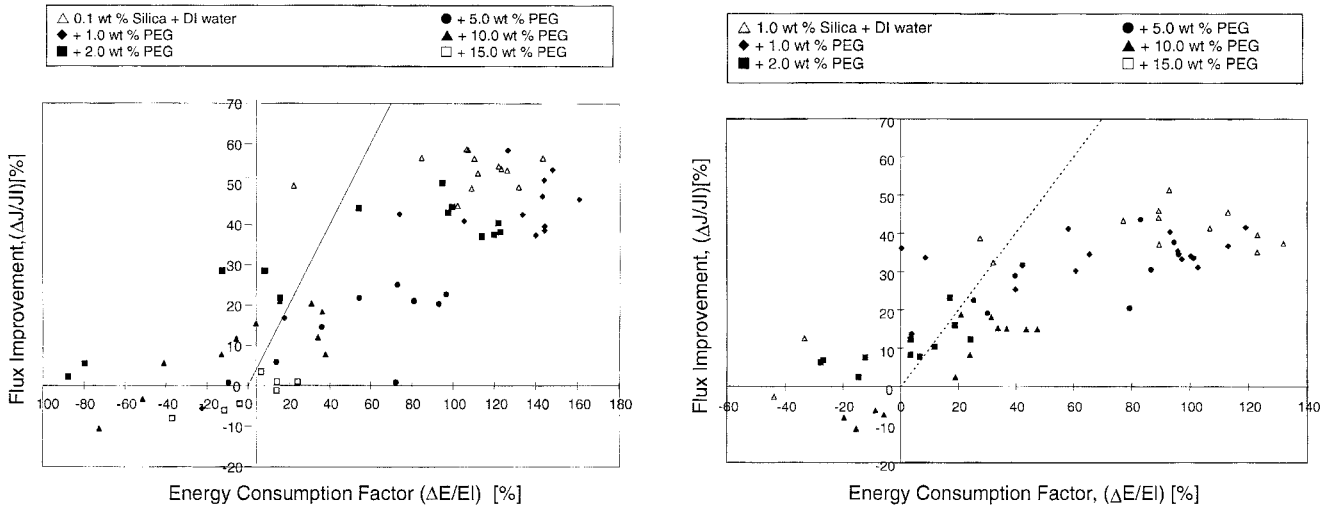

Figure 15. Flux improvement vs. energy consumption factor for different poly(ethylene) glycol solutions (c = 0–15.0 wt. %) containing (a) 0.1 wt. % and (b) 1.0 wt. % silica concentrations.

Open symbols represent data for the helical module and closed symbols represent the data for the linear module. (TMP = 27.58 kPa (4 psi), T = 27°C.)

the influence of viscosity from the x-axis (data not shown). These PEG solutions contained 0.1 and 1.0 wt. % silica concentrations. Again, for low PEG concentrations, the ratio follows the behavior of aqueous solution containing silica particles. With increasing *Re*, the ratio decreased from about 1 to about 0.6, and, for *Re* greater than 1,000 ($Q > 300$ mL/min) was relatively constant within an experimental error of $\pm 10\%$. However, with increasing PEG concentration, the influence of the viscous solutions on the resistance behavior became stronger and the ratio drop was less. With increasing PEG concentrations, the asymptotic resistance ratio (for $Q > 300$ mL/min) increased from 0.6 to 0.8 for PEG concentrations that increased from 2 to 10 wt. %.

Modeling

In Figure 16, the Sherwood number is plotted against the Reynolds number for PEG solutions containing 0.1 wt. % silica concentration for laminar flow in a linear (Figure 16a) and a helical module (Figure 16b). Notice how the correlations all have similar slopes for each design. The intercepts increase with suspension viscosity. For the helical system, the last few data points for each viscosity fluid exhibit lower Sherwood numbers than expected by the linear curve. Dampening of fluid instabilities could have caused this especially near the intermediate flow region. New mass-transfer correlations were obtained with respect to the solution viscosity. The diffusion coefficients used for silica were calculated according to the Stokes-Einstein equation (Eq. 6). The Sherwood numbers for the experimental data were estimated by replacing k with J (Eq. 5). Then they were compared with the correlation for laminar flow in a straight tube (see Rautenbach, 1997; Zeman and Zydney, 1996). As a first approximation, the concentration at the membrane surface was estimated to be roughly 40% for the linear and the helical module in all experiments. For the correlations described by Eq. 7, the pre-exponent (α) and the power exponents (b and c) were constant over the operational range of viscosity.

Helical Module

$$Sh = (0.01523) \times \left(\frac{a}{r_c}\right)^{0.07} \times Re^{0.55} \times Sc^{0.6124} \quad \text{for } c_{\text{silica}} = 0.1 \text{ wt. \%} \tag{18}$$

Linear Module

$$Sh = (0.07141) \times Re^{0.33} \times Sc^{0.5589} \quad \text{for } c_{\text{silica}} = 0.1 \text{ wt. \%} \tag{19}$$

The power exponents of 0.33 and 0.5589 for the linear module accounts for the increased viscosity of the suspensions and differs from the well-known behavior for laminar flow ($Re^{1/3} * Sc^{1/3}$) (Leveque, 1928), while the power exponents 0.07 and 0.55 for the helical module was the same as that predicted by Gehlert et al. (1998). The main difference was due in the power exponent for the *Sc* number of 0.6124 to account for the large increase in viscosity. All the data for 0.1 wt. % silica are compared with the predictive models (Eqs. 18 and 19) in Figure 17. The linear correlation fits were $R^2 = 0.9936$ and 0.9867 for the linear and helical modules, respectively.

Conclusions

In separate microfiltration experiments, permeation flux measurements of feeds containing (i) increasing polyethylene

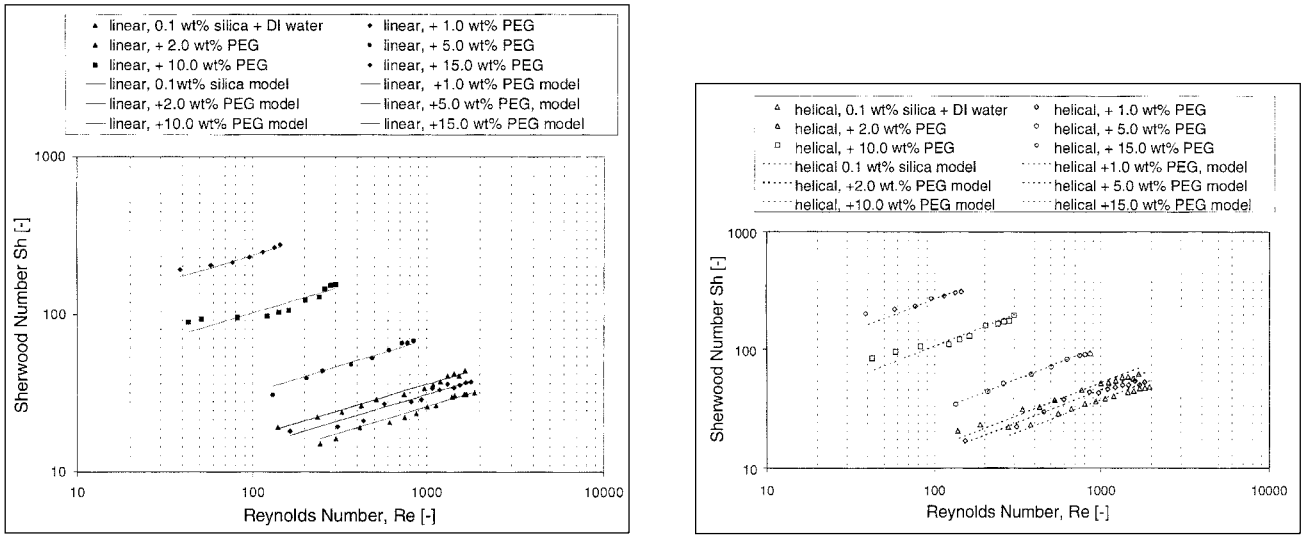

(a) **(b)**

Figure 16. Sherwood number vs. Reynolds number for different poly(ethylene) glycol suspensions (c = 0–15 wt. %) containing 0.1 wt. % silica concentration in (a) the linear module (solid symbols), and (b) the helical module (open symbols).

Solid and dashed lines describe Eq. 19 and Eq. 18 for the linear module and helical modules, respectively. (TMP = 27.58 kPa (4 psi), T = 27°C.)

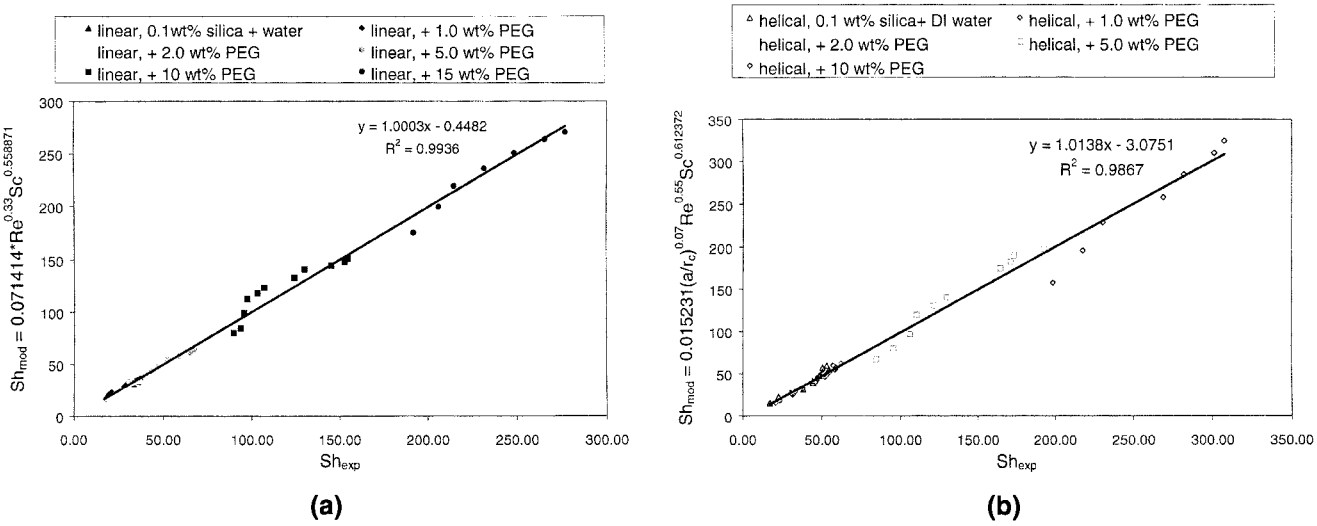

Figure 17. Comparison of the best fit correlations (Eqs. 18 and 19) vs. the observed data for the (a) linear and (b) helical modules.

The feed contained 0.1 wt. % silica particles and 0–15 wt. % PEG.

glycol concentrations without silica, (ii) increasing silica particle concentrations without polyethylene glycol, and (iii) mixtures of silica suspensions in PEG solutions were obtained. Conclusions from these experiments are summarized below.

For the feed with PEG and no silica particles, the permeate flux decreased according to the resistance model as a function of the inverse viscosity, but was independent of the Reynolds number. Both helical and linear modules performed similarly, as expected, since no flux improvement was observed (or expected). For the same range of axial-flow rates, the *Re* operating range decreased with increasing viscosity due to the definition of the *Re* number. The energy consumption was a strong function of viscosity. With increasing viscosity, the differences in energy consumption between flow in the helical and the linear module narrowed considerably, possibly due to the weaker Dean vortices at higher viscosities (*Re* were lower and hence, the operating range closer to the Re_c). The energy consumption increased with increasing Reynolds number, due to the higher axial pressure drop in both modules; however, because of the secondary flow in the helical module, additional pressure drop was observed.

For the feed with silica particles and no PEG, particle deposition or cake formation reduced the flux in the helical and the linear modules and affected the formation and stability of the Dean vortices. Because of their size ($> 0.5\ \mu$m), the particles were completely retained by the membrane (mean pore size 0.1 μm). The permeate flux increased with increasing *Re* and decreased with increasing silica concentration due to particle deposition on the membrane. In all cases the helical module performed better than the linear module due to the presence of the Dean vortices that reduced the cake resistance. Flux improvements of about 45% for all silica suspensions above a Reynolds number of 600 was observed. Due to negligible increases in viscosity through the addition of silica particles only, the energy consumption behavior as a function of Reynolds number was similar to that observed for pure water permeation. Thus, silica particle concentration (up to 1 wt. %) had a small noticeable effect on the energy consumption behavior. For $Re > 600$, the energy consumption factor (helical over linear) was found to be 120% for all silica concentrations. Table 3 summarizes the fitted parameters from Eq. 7 for silica suspensions only.

Comparative microfiltration experiments with PEG and silica particles in the feed show that flux improvements obtained with silica suspensions for Dean vortex as compared with cross-flow declined with increasing solution viscosity (or polyethylene glycol concentration). As the viscosity was increased from 1 cp to 12 cp, the flux improvement declined from $\sim 45\%$ to close to zero. The difference in energy consumption between flow in the helical with that in the linear module declined from 120% to 0% with a 12 fold increase in viscosity. Although flux improvements (helical over linear) were substantial for all silica suspensions with and without PEG, the energy required to obtain these increased fluxes was considerable. Energy and pressure drop predictions using the equations in the theoretical section were tested for several PEG and silica concentrations. The agreement was quite good in most cases. For high value (low volume) products like pharmaceuticals, food, and beverages, improved yield

Table 3. Mass-Transfer Parameters for Laminar Flow in a Linear and a Helical Module as a Function of Silica Concentration in Various Silica Suspensions*

Module	Silica Conc. (wt. %)	α	b	c	g	Ref.
Linear	0.05–1.0	0.2	0.45	0.25	0.0	This work
	3.0	0.1	0.62	0.22	0.0	This work
Helical	0.05–1.0	0.19	0.55	0.25	0.07	This work
	3.0	0.2	0.62	0.22	0.07	This work
	Dextran T500†	0.173	0.55	0.33	0.07	Gehlert et al. (1998)

*The constants are from Eq. 20.
†Dextran T500 (500 kDa) solutions (Gehlert et al., 1998).

and purity is paramount and the added expense of increased energy is of little importance. For low value (high volume) products such as for wastewater treatment, an additional significant pumping cost could be prohibitive.

Mass-transfer correlations that account for increasing viscosity were obtained after both Dean vortex and cross-flow. They are given by the general axial expression, viz.

$$Sh = \alpha\, Re^{b} Sc^{c} \left(\frac{a}{r_c} \right)^{g} \tag{20}$$

where α, b, and c are given in Eqs. 18 and 19 and $g = 0.07$ and 0.00 for the helical and linear modules, respectively.

The results presented here clearly identify the range of viscosity in which Dean vortices were effective in improving flux over that of cross-flow. The mass-transfer correlations could be used to estimate the absolute permeation flux and the flux improvement expected between Dean vortex flow and cross-flow with good confidence ($R^2 > 0.987$).

Acknowledgments

The authors thank Millipore Corporation, MA for partial funding and Vinay Goel, Steven Pearl, Stephen Dzengeleski, and Ralph Kuriyel for providing the membrane modules. Also we would like to thank Mr. Steven Modory at Degussa Corporation, OH for measurements of the silica particle-size distribution.

Notation

A = (external) membrane (surface) area, m^2, mm^2
A = mass-transfer parameter
B = mass-transfer parameter
c = concentration, wt. %, g/L
C = mass-transfer parameter
d = tube diameter, mm
d_i = inner diameter of the hollow fiber, mm
d_o = outer diameter of tube, mm
d_{rod} = diameter of the rod, mm
D = diffusion coefficient, m^2/s
E = energy consumption per unit area, W/m^2
J = permeate flux, $L/(m^2 h)$
L = membrane thickness, m
m = number of coils lying next to each other
Q = (volumetric) axial-flow rate, mL/min
r = radius of curvature, mm
r_s = radius of the solute particle, cm
t = (filtration) time, s
t = wall thickness of fiber, mm
TMP = transmembrane pressure, kPa
v = velocity, m/s
v_m = mean azimuthal or average velocity, m/s
V = volume, l, m^3
Δp_{TMP} = transmembrane pressure, kPa, psi
α = preexponent
η_r = ratio of dynamic viscosities
η' = radius ratio, $(r + a)/(r + a + t)$
π = osmotic pressure, kPa

Subscripts

b = bulk
c = cake layer (including concentration polarization and fouling)
h, hel. = helical, with Dean vortices
i = inlet
l, lin. = linear, without Dean vortices
o = outlet
p = permeate
s = solute
TMP = transmembrane
w = water

Literature Cited

Belfort, G., M. Brewster, and K.-Y. Chung, "Curved Channel Membrane Filtration," U.S. Patent No. 5,204,002 (Apr. 20, 1993).
Belfort, G., "Coiled Membrane Filtration System," U.S. Patent No. 5,626,758 (1997).
Brewster, M. E., K.-Y. Chung, and G. Belfort, "Dean Vortices with Wall Flux in a Curved Channel Membrane System: 1. A New Approach to Membrane Module Design," *J. Membrane Sci.*, **81**, 127 (1993).
Bubolz, M., M. Wille, G. Langer, and U. Werner, "Contributions to the Influence of Dean-Vortices on Crossflow Filtration," *F&S Filtrieren und Separieren*, **12**, 16 (1998).
Chung, K.-Y., M. E. Brewster, and G. Belfort, "Dean Vortices with Wall Flux in a Curved Channel Membrane System: 2. The Velocity Field in a Spiral Channel," *AIChE J.*, **42**, 347 (1995).
Chung, K.-Y., M. E. Brewster, and G. Belfort, "Dean Vortices with Wall Flux in a Curved Channel Membrane System: 3. Concentration Polarization in a Spiral Reverse Osmosis Slit," *Chem. Engr. J. Japan*, **31**, 683 (1998).
Dean, W. R., "Fluid Motion in a Curved Channel," *Proc. Roy. Soc. London A*, **121**, 402 (1928).
Gehlert, G., S. Luque, and G. Belfort, "Flux Enhancement Due to Secondary Flow in a Helical Tubular Module: 14 Ultra and Microfiltration of Polysaccharides, Proteins and Yeast Suspensions," *Biotechnology Papers*, **14**, 931 (1998).
Gnielinski, V., "Correlations for the Pressure Drop in Helically Coiled Tubes," *Verfahrenstechnik*, **17**, 683 (1983).
Kluge T., "Microfiltration of Biological and Other Solution Using Dean Vortices," Diplomarbeit, Technische Universitat Hamburg-Harburg, Germany (1998).
Leveque, M. D., "Lelois de la Transmission de la Chaleur par Convection," *Ann. Mines*, **13**, 201 (1928).
Luque, S., H. Mallubhotla, G. Gehlert, R. Kuriyel, S. Dzengeleski, S. Pearl, and G. Belfort, "A New Coiled Hollow Fiber Module Design for Enhanced Microfiltration Performance in Biotechnology," *Biotechn. Bioengr.*, in press (1999).
Mishra, P., and S. N. Gupta, "Momentum Transfer in Curved Pipes: 1. Newtonian Fluids," *Ind. Eng. Chem. Proc. Des. Dev.*, **18**, 130 (1978).
Moulin, R., J.-C. Rouch, C. Serra, M. J. Clifton, and P. Aptel, "Mass Transfer Improvements by Secondary Flows in Membrane Operations," *J. Membr. Sci.*, **114**, 235 (1996).
Rautenbach, R., *Membranverfahren, Grundlagen der Modul- und Anlagenauslegung*, Springer-Verlag, Berlin (1997).
Ramshankar, R., and K. R. Sreenivasan, "A Paradox Concerning the Extended Stokes Series Solution for the Pressure Drop in Coiled Pipes," *Phys. Fluids*, **31**, 1339 (1998).
Taylor, G. I., "Stability of Viscous Liquid Contained Between Two Rotating Cylinders," *Phil. Trans. Roy. Soc. A*, **223**, 289 (1923).
Wille, M., G. Langer, S. Geisler, and U. Werner, "Enhanced Efficiency for Crossflow Microfiltration with Capillary Membranes," *F&S Filtrieren und Separieren*, **10**, 112 (1996).
Zeman, L. T., and A. L. Zydney, *Microfiltration and Ultrafiltration: Principles and Applications*, Marcel Dekker, New York (1996).

Manuscript received Nov. 3, 1998, and revision received June 7, 1999.